A tenuous dust ring of Jupiter formed by escaping ejecta from the Galilean satellites

Alexander V. Krivov,[1,2] Harald Krüger,[3] Eberhard Grün,[3]
Kai-Uwe Thiessenhusen,[4] and Douglas P. Hamilton[5]

Received 29 November 2000; revised 16 October 2001; accepted 23 October 2001; published 25 January 2002.

[1] This paper focuses on the dust environment between the orbits of the Galilean moons of Jupiter. Recent discovery of dust clouds around the Galilean satellites formed by impact ejecta from hypervelocity impacts of interplanetary micrometeoroids [*Krüger et al.*, 1999d] suggests that a fraction of the ejected particles may escape from the source satellites into circum-Jovian orbits. We estimate production rates and study dynamical evolution of the escaping ejecta, controlled by gravitational, radiation pressure, and electromagnetic forces, to show that grains larger than several tenths of a micrometer in radius are likely to stay in bound orbits around Jupiter for tens or hundreds of years until they either are lost to collisions with the satellites or Jupiter or are ejected to interplanetary space. It is concluded that these small debris form a broad dust ring with number densities up to $\sim 10^3$ km^{-3}, extending at least from Europa's orbit outward beyond the orbit of Callisto. Our results are consistent with in situ measurements of the Galileo spacecraft. We analyze impact events recorded by the Galileo dust detector from 1996 through 2001 and find more than 200 events outside the orbit of Europa, compatible with impacts of particles orbiting Jupiter in prograde orbits. An empirical dust number density distribution derived from these data agrees quite well with the theoretical one. *INDEX TERMS:* 6213 Planetology: Solar System Objects: Dust, 6218 Planetology: Solar System Objects: Jovian satellites, 6265 Planetology: Solar System Objects: Planetary rings, 6035 Planetology: Comets and Small Bodies: Orbital and rotational dynamics; *KEYWORDS:* Cosmic dust, Jupiter rings, Galilean satellites, planetary magnetospheres, orbital dynamics, Galileo mission

1. Introduction

[2] Ring systems formed by tiny dust grains surround all giant planets of our solar system. Jupiter, the largest of the giants, is shrouded in diverse dust structures: the main ring and its vertically extended halo, the two extended gossamer rings [*Burns et al.*, 1999], escaping streams composed of tiny high-speed particles [*Grün et al.*, 1998], and electromagnetically captured interplanetary grains [*Colwell et al.*, 1998]. Formation of the gossamer rings, and presumably of the main ring, is explained by micrometeoroidal bombardment that ejects material off the small satellites [*Burns et al.*, 1999]. The same mechanism works for larger moons as well: tenuous impact-generated clouds have been recently discovered around Europa, Ganymede, and Callisto [*Krüger et al.*, 1999d]. In contrast to the debris of smaller inner moons, most of the particles lofted from the Galileans move in ballistic trajectories and fall back to the surfaces. Still, a certain fraction of them may escape from the source satellites into circum-Jovian orbits. In this paper we investigate how much ejecta could escape from the source satellites into the circum-Jovian space, their typical dynamics and lifetimes, and their steady state distribution in the Jovian system. Ultimately, we argue that these dusty debris create a tenuous ring around Jupiter detectable by in situ dust measurements.

[3] Another motivation for this work is provided by the data of the dust detector system (DDS) on board the Galileo spacecraft. Galileo has been in orbit about Jupiter since December 1995 and in the meantime has successfully completed more than 30 orbits about the planet. Galileo is equipped with a highly sensitive impact ionization dust detector which measures submicrometer and micrometer-sized dust grains [*Grün et al.*, 1992]. Since the beginning of Galileo's orbital tour about Jupiter (among other significant populations of dust) the dust detector has measured hundreds of impacts of micrometer-sized grains between the orbits of the Galilean satellites [*Grün et al.*, 1998; *Krüger et al.*, 1999a]. It has been suspected that many of these particles may come from the Galilean moons [*Thiessenhusen et al.*, 2000], although specific arguments have not been adduced yet. Therefore we perform a detailed analysis of these dust impacts and compare the dust distribution derived from the data to that predicted by the model.

[4] In section 2 we estimate the production rates of the escaping dust from Europa, Ganymede, and Callisto, study the dynamics of grains under the combined action of gravitational, radiative, and electromagnetic forces, and then derive the expected spatial distribution of these ejecta in the Jovian system. In section 3 we analyze relevant data of the Galileo dust detector, construct an empirical distribution of dust in the same region, and then compare the modeled and empirical distributions. Section 4 contains our conclusions and a discussion.

2. Model

2.1. Production Rates of Escaping Dust

[5] We start with the Galileo dust detections made during flybys near Ganymede [*Krüger et al.*, 1999d, 2000], Europa, and Callisto

[1]Institut für Physik, Universität Potsdam, Potsdam, Germany.
[2]On leave from Astronomical Institute, St. Petersburg University, St. Petersburg, Russia.
[3]Max-Planck-Institut für Kernphysik, Heidelberg, Germany.
[4]Institut für Biochemie, Charité, Humboldt-Universität zu Berlin, Berlin, Germany.
[5]Department of Physics and Astronomy, University of Maryland, College Park, Maryland, USA.

0148-0227/02/2000JE001434$09.00

Table 1. Estimated Dust Production Rates and Grain Lifetimes[a]

Sizes, μm	N^+_{esc}, s^{-1}	T, years	N
	Europa		
0.3 ... 0.6	1×10^{12}	90	3×10^{21}
0.6 ... 1.0	2×10^{11}	70	4×10^{20}
1.0 ...	7×10^{10}	70	2×10^{20}
	Ganymede		
0.3 ... 0.6	3×10^{12}	90	6×10^{21}
0.6 ... 1.0	4×10^{11}	60	8×10^{20}
1.0 ...	2×10^{11}	90	6×10^{20}
	Callisto		
0.3 ... 0.6	2×10^{12}	60	3×10^{21}
0.6 ... 1.0	2×10^{11}	30	2×10^{20}
1.0 ...	1×10^{11}	30	1×10^{20}

[a] N^+_{esc} is the production rate of escaping grains from the whole surface of a satellite, derived from the Galileo dust detections close to the moons. T is the mean lifetime of the particles in orbits about Jupiter, found from numerical simulations. $N = N^+_{esc} \times T$ is a steady state number of grains in the ring.

(H. Krüger et al., manuscript in preparation, 2002). The number densities $n(r)$ (r is the distance from the center of a satellite) derived from the Galileo data allow us to estimate the production rate of escaping grains from a moon as

$$N^+_{esc} \approx n(r) \times \eta_{esc}(r) \times 4\pi r^2 \times \bar{u}(r). \quad (1)$$

Here η_{esc} is the fraction of escaping grains among the particles at a distance r, and $\bar{u}$ is the mean velocity of the escaping grains at the same distance. Note that although all right-hand-side terms in (1) are distant-dependent, their product N^+_{esc} is independent of r.

[6] Analyzing the Galileo detector data during the spacecraft flybys near Ganymede, *Krüger et al.* [1999d, 2000] derived the dust number density in the distance range from 1.1 to $\sim 10R_s$, R_s being the satellite radius. For instance, $n(r) = 3 \times 10^4$ km^{-3} at $r = 3R_s$. The same procedure gives $n(r)$ for the dust clouds of Europa and Callisto (H. Krüger et al., manuscript in preparation, 2002); e.g., $n(r) = 2 \times 10^4$ km^{-3} at $r = 3R_s$ for Europa, and $n(r) = 1 \times 10^4$ km^{-3} at $r = 3R_s$ for Callisto.

[7] The mean velocity of the escaping grains at a distance r is roughly given by $\bar{u} \sim u_{esc}\sqrt{R_s/r}$, u_{esc} being the escape velocity from the satellite surface (2.0, 2.7, and 2.5 km s^{-1} for Europa, Ganymede, and Callisto, respectively).

[8] The fraction of escaping grains is given by

$$\eta_{esc}(r) = \frac{n_{esc}(r)}{n_{bound}(r) + n_{esc}(r)}, \quad (2)$$

where $n_{bound}(r)$ and $n_{esc}(r)$ are the number density of gravitationally bound and escaping grains at the distance r. Assuming that the ejecta speed distribution at the surface is approximated by a power law $\psi(>u) = (u_0/u)^\gamma$, *Krüger et al.* [2000] found analytic expressions for $n_{bound}(r)$ and $n_{esc}(r)$ (their equations (11) and (15)). The equations show that η_{esc} depends neither on the lower cutoff velocity u_0 nor on the escape velocity u_{esc} and that η_{esc} depends on the distance through the ratio r / R_s only. Therefore, for a given r / R_s, η_{esc} is the same for all satellites. We calculated η_{esc} from (11) and (15) of *Krüger et al.* [2000]. Over a plausible range $1.2 \le \gamma \le 2.0$ [*Krüger et al.*, 2000] the result is $\eta_{esc} = 0.10$ to 0.15 at $r = 2R_s$, $\eta_{esc} = 0.18$ to 0.25 at $r = 3R_s$, and $\eta_{esc} = 0.30$ to 0.38 at $r = 5R_s$.

[9] Equation (1) gives the cumulative production rate of all grains above the Galileo DDS threshold during the satellite flybys (with masses $m_g \gtrsim 10^{-13}$ g or with radii $r_g \gtrsim 0.3$ μm). To calculate the production rates in different size intervals, we apply the mass distribution $N^+_{esc}(>m_g) \propto m_g^{-\alpha}$ with $\alpha = 0.8$. This value is compatible with the Galileo flyby data that give slopes between 0.6 and 1.0 [*Krüger et al.*, 1999d] as well as with the impact experiment data [see, e.g., *Asada*, 1985; *Kato et al.*, 1995, and references therein].

[10] The derived values N^+_{esc} are listed in Table 1, which shows that all three moons have comparable efficiencies as sources of dust, ejecting $N^+_{esc} \sim 10^{12}$ particles, or $\sim 10^2$ grams of material per second into the Jovian system. Of course, all these estimates are very rough. Lack of laboratory data on ejecta speed distributions at high-velocity range ($\gtrsim 2$ km s^{-1}) makes the factor η_{esc} uncertain by at least 1 order of magnitude. Since the number densities $n(r)$ taken from the Galileo data have ~ 1 order of magnitude uncertainty, the values N^+_{esc} given in Table 1 may be uncertain by at least a factor of 30. We emphasize, however, that this way of estimating the production rate of escaping grains, which makes use of the Galileo flyby data, is less uncertain and more reliable than modeling the projectile fluxes and impact ejecta production [*Krüger et al.*, 2000] because such models contain a number of poorly constrained parameters (impactor flux, ejecta yield, ejecta mass distribution, etc.).

2.2. Forces Acting on the Grains

[11] Having set the initial conditions at the source moons, we consider the dynamics of the escaping ejecta in the circum-Jovian orbits. Apart from Jupiter's point-mass gravity, the dust particles experience four strong perturbing forces: (1) solar radiation pressure (RP), (2) perturbations from Jupiter's oblateness (J2), (3) the Lorentz force (EM) that stems from the Jovian magnetic field and electrostatic charges acquired by the grains in the Jovian magnetosphere, and (4) the gravity of the Galilean satellites (SG). Other perturbing forces and effects, such as the Poynting-Robertson drag, are not important; see a discussion in section 2.5.

[12] For a while, let us put aside the force 4, the satellite gravity, and estimate the relative importance of the forces 1–3 for different-sized grains released from different parent moons. For simplicity, we consider a spherical particle that moves in a prograde circular Keplerian orbit of radius r in the equatorial plane. We also assume a dipole aligned corotating magnetic field of the planet. Then the ratios of the perturbing forces (radiation pressure force F_{pr}, oblateness force F_{obl}, and Lorentz force F_{em}) to the planetary gravity force F_{gr} are estimated as

$$\frac{F_{pr}}{F_{gr}} = \frac{3}{4} Q_{pr} \frac{F_\odot r^2}{GMc\rho_g r_g}, \quad (3)$$

$$\frac{F_{obl}}{F_{gr}} = \frac{3}{2} J_2 \left(\frac{R}{r}\right)^2, \quad (4)$$

$$\frac{F_{em}}{F_{gr}} = |L|\left|1 - \frac{n}{\Omega}\right|, \quad L \equiv \frac{Q_g B_0 R^3 \Omega}{GMcm_g}. \quad (5)$$

Here GM is the gravitational parameter of the planet, Q_{pr} is the radiation pressure efficiency factor, $F_\odot$ is the solar flux at the heliocentric distance of the planet, c is the speed of light, r_g and ρ_g are the radius and bulk density of the grain, m_g and Q_g are its mass and charge, J_2 and R denote the second zonal harmonic coefficient and the equatorial radius of the planet, respectively, Ω is the angular velocity of the planet's rotation, B_0 is the magnetic field strength at the planetary equator, and $n = \sqrt{GM/r^3}$ is the mean motion of the particle. The Lorentz force naturally decouples to the "electric" part F_e, arising from the corotational electric field, and

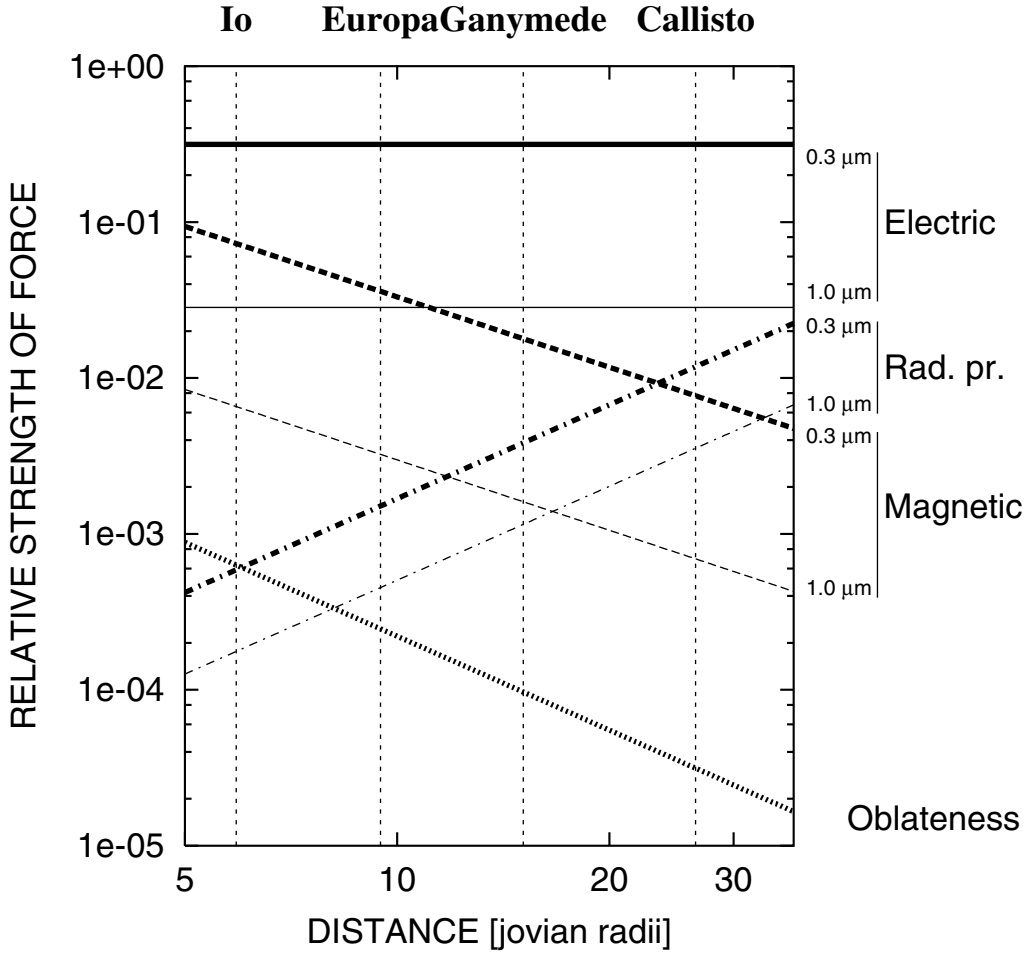

Figure 1. Strengths of the perturbing forces (radiation pressure, planetary oblateness, and the electric and magnetic components of the Lorentz force) acting on 0.3- (bold lines) and 1-μm-sized (thin lines) spherical icy grains, as functions of distance from Jupiter. Solid lines, electric force; dashed, magnetic force; dash-dotted, radiation pressure; dotted, oblateness. Depicted are the ratios of the forces to the Jovian point-mass gravity force.

the "magnetic" part F_m [*Hamilton*, 1993]. Accordingly, (5) can be replaced with expressions

$$\frac{F_e}{F_{\rm gr}} = |L| \quad \text{and} \quad \frac{F_m}{F_{\rm gr}} = |L|\frac{n}{\Omega}. \tag{6}$$

[13] For the sake of numerical estimates, we assume ρ_g = 1 g cm^{-3} and $Q_{\rm pr}$ = 1. In CGS-ESU units, the grain charge $Q_g = r_g\Phi/300$, where electrostatic surface potential Φ is measured in volts. We adopt a constant equilibrium value of +5 V [see *Horányi*, 1996, Figure 3; cf. *Burns et al.*, 1984, 1999]. Other parameters are $R = 7.134 \times 10^9$ cm, $GM = 1.266 \times 10^{23}$ cm^3 s^{-2}, $J_2 = 1.471 \times 10^{-2}$, $\Omega = 1.772 \times 10^{-4}$ s^{-1}, and B_0 = 4.2 G.

[14] Figure 1 gives the relative strengths (3), (4), and (6) of the forces as functions of the planetocentric distance r for grains with radii r_g = 1 and 0.3 μm. The forces vary with distance as $F_{\rm pr}/F_{\rm gr} \propto r^2$, $F_{\rm obl}/F_{\rm gr} \propto r^{-2}$, $F_e/F_{\rm gr} \propto r^0$, $F_m/F_{\rm gr} \propto r^{-3/2}$ and with the grain radius as $F_{\rm pr}/F_{\rm gr} \propto r_g^{-1}$, $F_{\rm obl}/F_{\rm gr} \propto r_g^{0}$, $F_e/F_{\rm gr} \propto r_g^{-2}$, $F_m/F_{\rm gr} \propto r_g^{-2}$. r_g^{-2}. The results show that for submicrometer-sized grains, especially ejected from inner Galilean satellites, the Lorentz force is the strongest perturbation, comparable in magnitude with the central gravity. For the dynamics of larger, 1-μm-sized grains, especially from Ganymede and Callisto, radiation pressure becomes important. Oblateness plays a minor role in the dynamics.

[15] The last perturbing force, the satellite gravity, is particularly important during occasional close encounters of the dust particles with the moons (cf. *Dobrovolskis et al.* [2000], who studied the problem without taking into account non-gravitational forces). It has an essentially stochastic nature, which does not allow us to estimate its effect on the dynamics in the same way as for the other forces.

2.3. Motion of Smaller Grains: Analytic Theory

[16] The estimates of the perturbing forces suggest that for ~0.3-μm-sized grains (comparable to the Galileo DDS detection threshold for impact speed of several km s^{-1}), ejected from Europa, the Lorentz force is by far the strongest perturbation. As we shall see below, these grains are expected to dominate the dust environment. Therefore considering this force alone may be a reasonable first approximation. To alleviate analytic derivations, we consider a two-dimensional (2-D) problem and assume a dipole magnetic field corotating with Jupiter: $\mathbf{B} = \mathbf{B}_0(R/r)^3$. Under these assumptions the equation of the grain motion in CGS-ESU units,

$$\ddot{\mathbf{r}} = -\frac{GM\mathbf{r}}{r^3} + \frac{Q_g}{m_g c}[\dot{\mathbf{r}} \times \mathbf{B} - (\boldsymbol{\Omega} \times \mathbf{r}) \times \mathbf{B}], \tag{7}$$

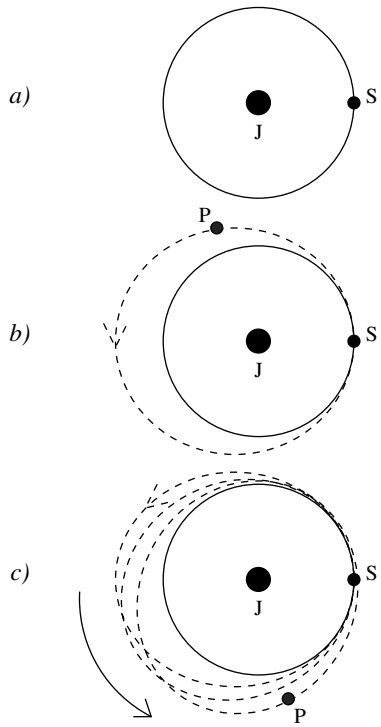

Figure 2. Release of a grain from a parent moon. *J* is Jupiter, *S* is the moon, and *P* is the grain. (a) The circular orbit and the position of the parent moon at the moment of release. (b) The elliptical initial orbit of the grain after release. The pericenter of the ellipse coincides with the launch point; the semimajor axis and eccentricity are determined by the corotating electric field. (c) Subsequent motion of the grain. The precession rate of the orbital ellipse is controlled by the magnetic part of the Lorentz force.

can be rewritten in the form

$$\ddot{\mathbf{r}} = -\frac{GM'\mathbf{r}}{r^3} + \frac{Q_g}{m_g c}[\dot{\mathbf{r}} \times \mathbf{B}], \tag{8}$$

where

$$M' \equiv M(1 - L) \tag{9}$$

and L is given by (5). Equation (8) shows that, for equatorial orbits, the "electric" part of the Lorentz force effectively reduces the Jovian mass from M to M' but leaves the motion Keplerian. The only actual perturbation stems from the "magnetic" part of the Lorentz force, described by the second term in (8).

[17] The equation of motion (8) admits two integrals of the motion, the energy integral [*Hamilton and Burns*, 1993]

$$\frac{\dot{\mathbf{r}}^2}{2} = \frac{GM'}{r} + \text{const} \tag{10}$$

and momentum integral

$$\mathbf{r} \times \dot{\mathbf{r}} = \frac{Q_g \mathbf{B}_0 R^3}{GMcr} + \text{const}, \tag{11}$$

so that the problem is integrable in quadratures.

[18] Consider a moon (Europa, Ganymede, or Callisto) moving about Jupiter in a circular orbit ($e_0 = 0$) with semimajor axis a_0, and a dust grain that escapes from the moon with a negligibly small initial velocity at the "local infinity." What orbital elements a, e will the grain have initially? As the particle rapidly acquires a positive electric charge, it feels the reduced inward acceleration of a planet with effective mass M'. This results in an outward shift of the orbit, an effect first discussed by *Schaffer and Burns* [1987]. We note that a similar effect occurs for a dust grain released from a comet or asteroid which immediately feels an effective solar mass $M' = M(1 - \beta)$, where β is the radiation pressure to the solar gravity ratio [*Burns et al.*, 1979]. By direct analogy with well-studied cometary dust dynamics we find that the grain will have initial elements

$$a' = a_0 \frac{1 - L}{1 - 2L} \quad \text{and} \quad \mathrm{e}' = \frac{\mathrm{L}}{1 - \mathrm{L}}, \tag{12}$$

with the release point being the pericenter of the grain orbit (Figures 2 a and 2b.)

[19] From here on, we use primes to emphasize that a' and e' are osculating elements that assume the reduced central mass M' and hence differ from usual osculating elements a and e that refer to a central mass M. The modified elements a' and e' describe the exact Keplerian ellipse followed by a particle influenced both by gravity and by the electric part of the electromagnetic force (see equations (7) and (8)). These are by far the strongest two forces acting on a small dust grain around Jupiter (Figure 1). By basing our perturbation theory on the combined solution rather than on the gravity-only solution, as is commonly done, we are able to extend the validity of the perturbation approach to smaller grain sizes than would otherwise be possible. Moreover, our approach reduces the size of the perturbations for all grain sizes with the result that the primed elements vary more smoothly than the unprimed ones and are also more directly related to the actual geometry of the orbit. Replacing the physical mass of the planet with the reduced mass also affects two other osculating elements: the longitude of pericenter ($\tilde{\omega}' \neq \tilde{\omega}$) and the mean anomaly. The elements that determine the orientation of the orbital plane (the inclination and the longitude of the ascending node) are independent of the choice of the central mass: $i' \equiv i$ and $\Omega' \equiv \Omega$.

[20] If $L \geq 1/2$, the grain will be ejected out from the circum-Jovian space into interplanetary space on escape orbits [*Hamilton and Burns*, 1993]; this is the case for grains less than $\approx$0.24 μm in radius. It is this mechanism that produces the Jovian dust streams [*Horányi et al.*, 1993; *Grün et al.*, 1998]; only their source (Io) and their production mechanism (volcanoes) differ. When $L < 1/2$, the grain starts moving in elliptic orbit with orbital elements given by (12). The the "magnetic" part of the Lorentz force, i.e., the second term in (8), comes into play. It results in the precession of the orbital ellipse (Figure 2c). The precession rate can be found in the orbit-averaged approximation from the Gauss perturbation equations for (8):

$$\begin{aligned}\dot{\tilde{\omega}}' &= 2\frac{Q_g B_0}{m_g c}\left(\frac{R}{a'}\right)^3 \left(1 - e'^2\right)^{-3/2} \\ &= 2\frac{Q_g B_0}{m_g c}\left(\frac{R}{a_0}\right)^3 (1 - 2L)^{3/2}.\end{aligned} \tag{13}$$

Note that this equation has the same form as the expression for $\dot{\tilde{\omega}}$ [*Hamilton*, 1993]; primed quantities simply replaced unprimed ones. This follows from the fact that for equatorial orbits, the electric force causes no pericenter precession.

[21] Using the equations just derived and parameter values described above, one gets the following numerical results. For 0.3-μm grains lost by all three satellites, $L = 0.32$, $e' = 0.46$, and $a' = 1.86a_0$. This means that perijove and apojove of these grains are at $1.00a_0$ and $\approx 2.7a_0$, respectively, so that the Europa grains spread between the orbits of Europa and Callisto, and even

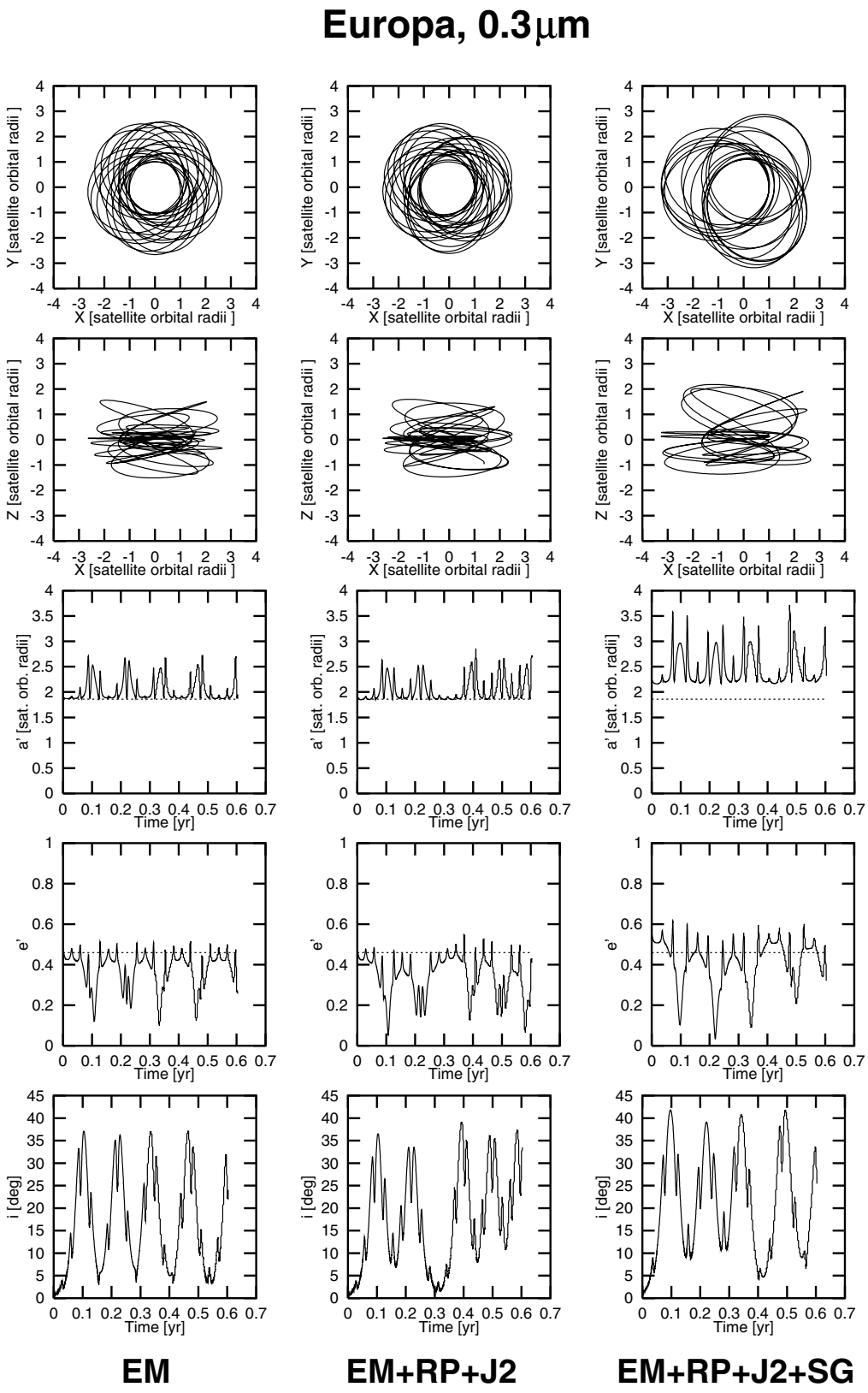

Figure 3. Dynamics of 0.3-μm Europa grains from numerical integrations. Jupiter's point-mass gravity is always included, and different sets of the perturbing forces are considered. Left column, the Lorentz force alone; middle column, the Lorentz force, radiation pressure, and Jovian oblateness acting together; right column, these forces plus the gravitational perturbations from the Galilean satellites. From top to bottom: trajectories in *XY* and *XZ* projections of the Jovian equatorial system; histories of the orbital elements a', e', and i. Horizontal dashed lines in the panels for a' and e' are constant values (equation (12)) predicted by a simplified analytic model. Note that the primed orbital elements a' and e' employ an altered central mass $M' = M(1 - L)$.

farther away from Jupiter. The rotation period of the line of apsides is 0.6, 2.4, and 13.2 years for 0.3-μm grains from Europa, Ganymede, and Callisto, respectively.

[22] To check these analytic results and to see whether the Lorentz force indeed dominates the dynamics of 0.3-μm-sized Europa grains, we undertook numerical integrations (described in detail in section 2.5). Figure 3 shows a typical trajectory and histories of the orbital elements of a single grain under the action of the Lorentz force alone (left column), of the EM, RP, and J2 forces (middle column), and of these forces plus satellite gravity (right column). First, a comparison of the left column in the figure to the other ones makes it clear that the RP and J2 forces are unimportant. Only the satellite gravity, which moderately broadens the orbital (and spatial) distributions of the Europa grains, is of some importance. Second, it is well seen that our simple analytic theory provides reasonable guidelines to the dynamical behavior: the trajectory is essentially a precessing ellipse with oscillating a' and e', the average values being reasonably close to $e' = 0.46$ and $a' = 1.86a_0$ as predicted above. The large periodic changes in inclination visible in Figure 3, which are correlated with the oscillations in a' and e', are intriguing. *Hamilton* [1993] derived the orbit-averaged equations for evolution due to the Lorentz force, and his equation for i has the form

$$\left\langle \frac{di}{dt} \right\rangle = \frac{1}{8} nL \frac{e^2}{\sqrt{1-e^2}} \sin(2i)\sin(2\omega), \tag{14}$$

where ω is the argument of pericenter. This equation predicts that initially uninclined orbits remain in the equatorial plane, and indeed they do for grains with $r_g > 0.35$ μm. For grains 0.35 μm and smaller, however, the perturbing Lorentz force is so strong that averaging over an unperturbed Keplerian orbit, as was done in the derivation of (14), is no longer a good approximation. Hence the above solution for di/dt begins to break down, and long-period large-amplitude oscillations in the inclination appear. The amplitude is strongly size-dependent, ranging from 15° for a 0.33 micrometer grain to 60° for a 0.26 μm grain.

2.4. Motion of Larger Grains: Semianalytic Study

[23] Still ignoring the satellite gravity, let us now turn to the more complex case when three perturbing forces (electromagnetic, radiative, and oblateness) act together. This problem, in 2-D and orbit-averaged approximations, and under some simplifying assumptions (circular orbit of a planet, absence of the planetary shadow, etc.), was investigated in depth by *Hamilton and Krivov* [1996]. They have shown that the grain semimajor axes have no secular changes and that the eccentricity e and the solar angle $\phi_\odot$ (the angle between the directions from the planet to the Sun and to the pericenter of the grain orbit) obey the equations

$$\frac{de}{d\lambda_\odot} = -\frac{\sqrt{1-e^2}}{e} \frac{\partial \mathcal{H}}{\partial \phi_\odot}, \quad \frac{d\phi_\odot}{d\lambda_\odot} = \frac{\sqrt{1-e^2}}{e} \frac{\partial \mathcal{H}}{\partial e}, \tag{15}$$

where

$$\mathcal{H} = \sqrt{1-e^2} + Ce\cos\phi_\odot + \frac{W}{3(1-e^2)^{3/2}} + \frac{\tilde{L}}{2(1-e^2)} \tag{16}$$

and $\lambda_\odot$ is the longitude of the Sun (a linear function of time). Here, C, W, and $\tilde{L}$ are size- and distance-dependent parameters that measure the strengths of the radiation pressure, oblateness, and Lorentz force, respectively; see *Hamilton and Krivov* [1996] for their exact definition. Using the integral of the motion,

$$\mathcal{H}(e, \phi_\odot) = \text{const}, \tag{17}$$

Hamilton and Krivov gave a detailed analysis of the solutions. They have shown, in particular, that the orbital eccentricities experience periodic oscillations and the lines of apsides librate or rotate, depending on the source moon and on the grains' sizes.

[24] Equations (15)–(17), which use the standard osculating elements, can be transformed into functions of the primed elements. The resulting expressions have the same functional form as above; only the constants C, W, and $\tilde{L}$ are altered. In equations (1)–(6) of *Hamilton and Krivov* [1996], which define these parameters, each of the unprimed elements and the central mass should be replaced by the corresponding primed quantity. Furthermore, the grain mean motion n should be replaced by $n' = \sqrt{GM'}a'^{-3/2}$. We now use the primed versions of (15)–(17) to estimate maximum eccentricities attained by dust grains of different sizes.

[25] In Figure 4 we show the initial eccentricities e' (equation (12)) as well as the maximum and minimum eccentricities attained by different-sized grains from the three source moons, found by numerical integrations of (15), rewritten in the primed elements. For brevity, we will call this technique semianalytic. Somewhat counterintuitively, typical eccentricities are not monotonic functions of grains' sizes. The grains just above ≈0.24 μm develop large eccentricities, close to unity. With increasing particle size, the eccentricities first decrease, then increase, reach a maximum value at several micrometers, and then decrease again. The jump in $e'_{\max}$ at several micrometers is not an artifact of the modeling; it is a real dynamical phenomenon that has been described in detail by *Hamilton and Krivov* [1996].

[26] Another message from Figure 4 is that typical eccentricities increase with the distance of a parent moon from Jupiter. While the Europa grains keep moderate eccentricities, the orbits of the Callisto grains are so eccentric that they are able to enter the innermost part of the Jovian system, where they can be easily lost owing to collisions with inner satellites, the main ring system, or even Jupiter's atmosphere.

[27] Altogether, ejecta in a broad size range, from several tenths to about 10 μm, especially those lost by Europa, develop inclinations and eccentricities large enough for the grains to avoid fast removal by reimpacts onto the parent moons. They spread widely between the satellites' orbits. Because smaller grains are ejected from the moons at higher rates than larger ones, we can expect the particles with several tenths of micrometers in size to prevail in the dust complex. Incidentally, the minimum size of the debris which we expect to dominate the system is close to the velocity-dependent detector threshold (≈0.3 μm for the impact velocities considered here). This favors identification of the ring particles in the spacecraft data.

2.5. Full Dynamics: Numerical Simulations

[28] Although the semianalytic results give us a good idea of the dynamics, we have yet to include the fourth perturbing force, the gravity of the satellites, and to consider a 3-D problem, to see how the dynamical picture is modified. For this purpose we undertake numerical integrations of Newton's second law $\mathbf{F} = m_g\ddot{\mathbf{r}}$. The equations of motion include Jupiter's gravity and the four forces listed above. The particles are assumed to be compact spheres of water ice with the radiation pressure efficiencies given by *Lamy* [1974]; for instance, $Q_{\rm pr} = 0.32$ for $r_g = 0.3$ μm. The Lorentz force is calculated for the equilibrium electrostatic surface potential of the grains of +5 V [cf. *Burns et al.*, 1999; *Horányi*, 1996; *Burns et al.*, 1984] and a corotating dipolar magnetic field of Jupiter with $B_0 = 4.2$ G, tilted by 9.6° to the planet's rotation axis. We neglect the plasma drag [*Burns et al.*, 1984] and Poynting-Robertson forces, which are of less importance over the time intervals considered. The effects of time-dependent charges due to gradients of the plasma density and temperature [*Horányi*, 1996] in the region of the Galilean moons are also small enough to be safely ignored. Perturbations from the solar gravity are very important far from

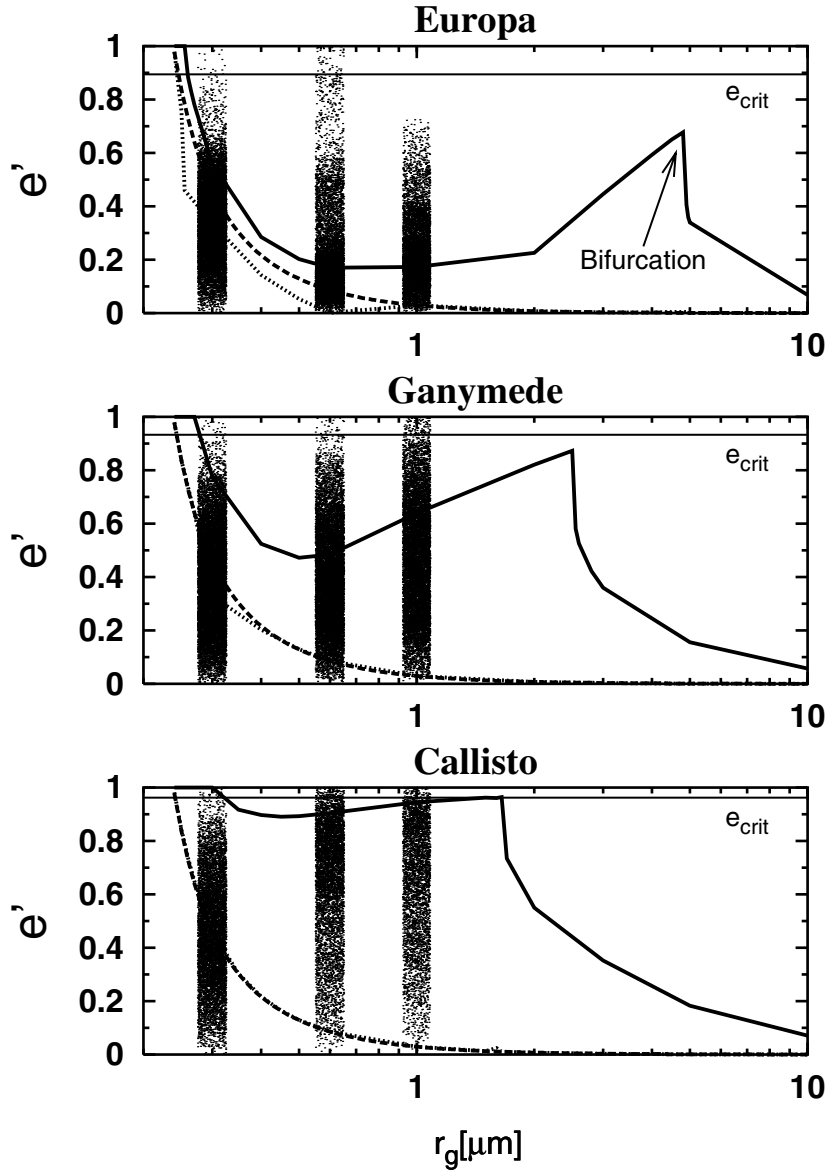

Figure 4. Typical orbital eccentricities of grains as functions of their sizes. The bold dashed line is the initial eccentricity of a grain released from a moon in a circular orbit (equation (12)). Bold solid (dotted) lines are the maximum (minimum) possible eccentricities in the orbit-averaged, 2-D problem with perturbations from the Lorentz force, radiation pressure, and planetary oblateness. These values were calculated by numerical integration of (15). These semianalytic results are to be compared to a more accurate dynamical model that describes a nonaveraged, 3-D problem with all the forces listed above plus the gravity of the Galilean satellites. Columns of dots show the instantaneous eccentricities of a large number of grains with sizes 0.3, 0.6, and 1.0 μm computed with this model (the columns were stretched horizontally to make the dots visible). Finally, horizontal thin solid lines depict critical eccentricity, for which a grain would strike Jupiter in pericenter of its orbit.

Jupiter, in the region of its outer satellites (from Leda to Sinope [see *Hamilton and Krivov*, 1996, Figure 1]), but can be safely neglected in the region of Galilean moons. The equations of motion of four Galilean satellites [*Lieske*, 1977], taking into account a triple resonance between Io, Ganymede, and Europa, were integrated simultaneously with the equation of motion of a dust grain. *Everhart* [1985] routine with the automatic choice of step size was used.

[29] In Figure 4 we have overplotted "exact" results, obtained by numerical integrations of the full equations of motion. Although the quantitative discrepancies between semianalytic and numerical results are large, the qualitative behavior is similar. Both the numerical simulations and the semianalytic model show that typical eccentricities are not monotonic functions of grain radii, and that the eccentricities increase with the distance of a parent moon from Jupiter. The analysis shows that grain dynamics cause ejected debris to smear out into a broad dust ring, numerically dominated by Europa grains several tenths of a micrometer in size.

[30] Some other integration results are shown in Figure 5, Figure 6, and Figure 7. Figure 5 depicts histories of a', e', and i of 0.3-μm Europa grains. Satellite gravity scatters the grains through numerous close encounters of the particles with the moons, broadening the distributions of semimajor axes and eccentricities with respect to distributions imposed by electromagnetic, radiative, and oblateness perturbations. Besides, the particles develop orbital inclinations up to several tens of degrees.

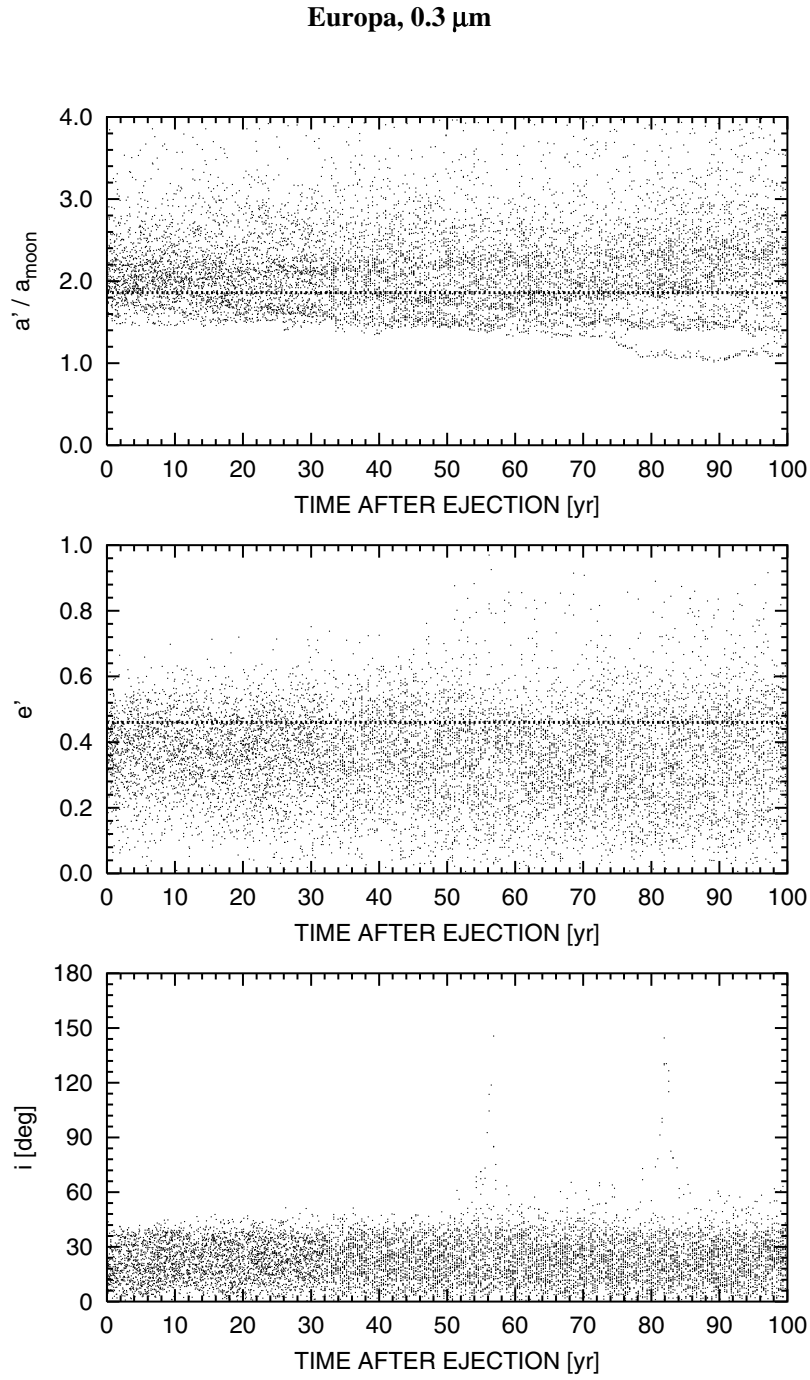

Figure 5. Instantaneous values of a', e', and i of 0.3-μm-sized grains ejected from Europa (dots). Typical a' and e' are close to the values given by (12) (horizontal lines).

[31] The scatterplots for the same grains in two projections, pole-on and edge-on, are presented in Figure 6, making it evident that these grains are widely scattered in the region between Europa and Callisto, forming a spherically symmetric ring with a non-negligible thickness. Figure 7 shows pole-on scatterplots (for 0.6 μm grains from Europa and Ganymede) for one particular Jovian season. While the ring of 0.3-μm grains is rotationally symmetric (Figure 6), because the dynamics of such small grains are dominated by the Lorentz force arising from a symmetric magnetic dipole, the ring composed of the 0.6-μm grains is no longer rotationally symmetric: the dust ring is displaced toward the Sun. This is an example of the radiation pressure effects. Similar phenomena were predicted for Saturn's E ring particles [*Horányi et al.*, 1992; *Hamilton*, 1993; *Hamilton and Krivov*, 1996] and for the ejecta from the Martian moon Deimos [*Hamilton and Krivov*, 1996; *Krivov and Hamilton*, 1997].

[32] In our problem the larger the grains and the more distant the parent moon, the greater the asymmetry: for instance, the asymmetry of a Callisto ring of 1.0-μm-sized grains is larger than that of the Ganymede 0.6-μm-sized ones. However, we shall see below that the contribution of larger particles to the overall number density is smaller than that of smaller grains and that Europa's grains make a

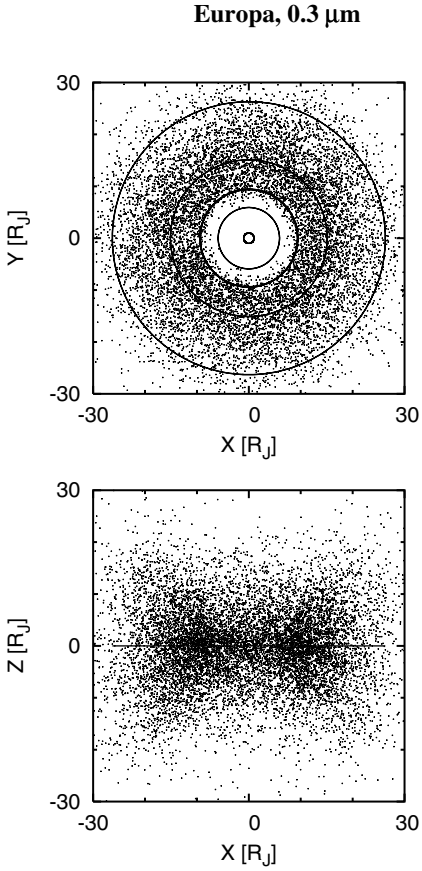

Figure 6. A dust ring composed of 0.3-μm-sized ejecta from Europa in (top) *XY* and (bottom) *XZ* projections of the Jovicentric equatorial equinoctal coordiante system (*X* axis is directed to the Jovian vernal equinox point, i.e., to the ascending node of the Jupiter orbital plane on the Jovian equatorial plane). In the top panel, circles mark Jupiter itself and the orbits of Io, Europa, Ganymede, and Callisto (thick circle shows the orbit of the parent satellite).

larger contribution than Ganymede and especially Callisto. That is why the asymmetry effects are extremely difficult to detect.

[33] We have also checked whether some grains are locked near the moons owing to the triple mean-motion resonance between the three inner Galileans or near the Lagrangian points. None of these effects were found.

2.6. Distributions of Dust

[34] To model the steady state spatial distribution of dust, we considered test particles with radii 0.3, 0.6, and 1.0 μm, as representatives of the size intervals [0.3, 0.6], [0.6, 1.0], and >1.0 μm (smaller particles in each interval dominate). The grains were launched from random points on the surfaces of Europa, Ganymede, and Callisto with initial speeds slightly in excess of the escape velocities of the source moons. The Jovian season, i.e., the longitude of the Sun at the moment of ejection, which determines the direction of the radiation pressure force, was chosen randomly. For each moon and grain size, 20 trajectories were integrated, and up to 70,000 modeled instantaneous positions of grains were collected. We distributed these positions into uniformly chosen bins of planetocentric distance and obtained spatial number density distributions for all sorts of grains (in arbitrary normalization).

[35] In the same numerical integrations, we determined the lifetimes of the grains by checking the position of a grain with respect to the moons and Jupiter. The lifetimes of individual grains differ considerably; 3 out of 180 test particles reimpacted their parent moons in <1 year, while 88 survived for more that 100 years. The survival time of micrometer-sized particles is also limited by plasma sputtering and micrometeoroidal bombardment [*Burns et al.*, 1984], effects which may destroy grains on timescales of hundreds to thousands of years. The surface erosion rate of 10^{10} to 10^{8} mol cm^{-2} s^{-1} for Europa [*Johnson et al.*, 1983] gives similar estimates for lifetimes of 0.3-μm-sized Europa grains against sputtering: ~30 to 3000 years. Sublimation can be efficient at 5 AU from the Sun only for purely icy grains, whereas the Galilean ejecta are likely to be contaminated with nonicy constituents [see, e.g., *Showman and Malhotra*, 1999 and references therein]. Thus these mechanisms are probably less important than dynamical sinks considered here. From our simulations the average lifetimes were found to be several tens of years (Table 1), or ~10^{3} to 10^{4} revolutions about Jupiter. They are limited by grain reimpacts with a parent moon (Europa's grains), collisions with a parent or another Galilean moon (dust from Ganymede), and collisions with Jupiter or escapes (Callisto's dust). We do not give statistics of the ejecta lifetimes and fates, because the number of simulated trajectories (180) is not large enough for this purpose.

[36] Finally, for the three source moons and three size intervals, we computed steady state numbers *N* of grains in the system (Table 1). These numbers were applied to convert the arbitrarily

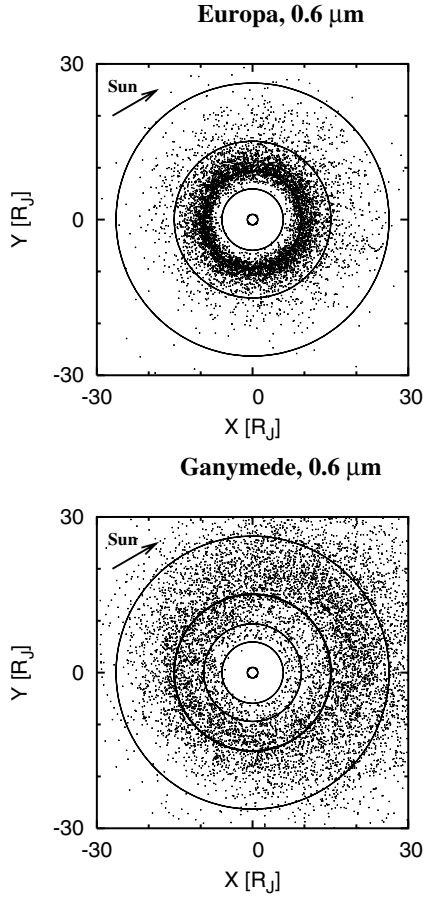

Figure 7. Dust rings formed by 0.6-μm-sized ejecta from (top) Europa and (bottom) Ganymede in *XY* projection of the Jovicentric equatorial equinoctal coordinate system. Shown are the views of the rings for one particular season: Jovian spring, shortly after the vernal equinox (direction toward the Sun is indicated). Circles have the same meaning as in Figure 6.

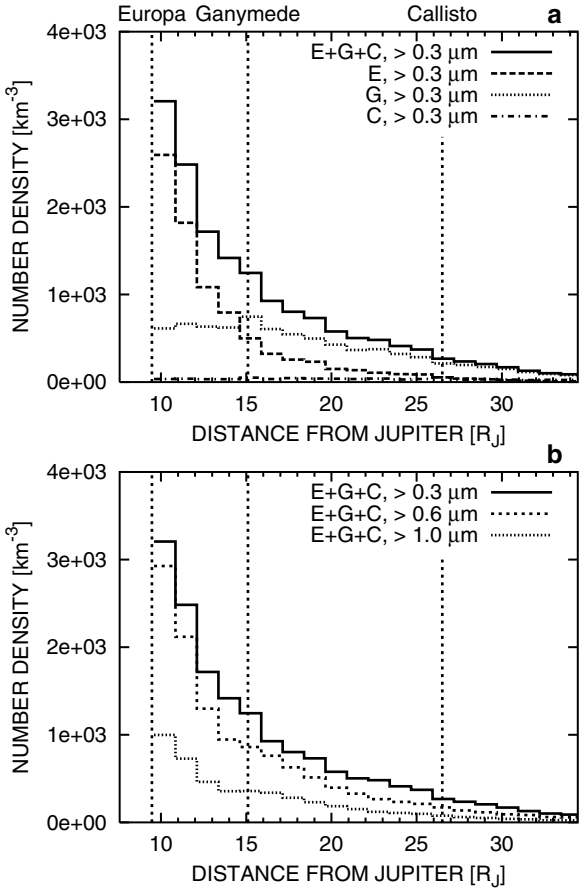

Figure 8. Number density distributions of escaping ejecta from the Galilean moons predicted by the model. (a) Partial contributions to the number density of the >0.3-μm grains made by the ejecta from Europa (dashed line), Ganymede (dotted line), and Callisto (dash-dotted line) alone and their sum (solid line). (b) Partial contributions made by the ejecta with radii >1 μm (dotted line), >0.6 μm (dashed line), and >0.3 μm (solid line) from three outer Galileans together. Solid lines in both panels are the same.

normalized spatial distributions of dust to the absolute number densities of different-sized grains at various distances from Jupiter.

[37] Figure 8 depicts the estimated absolute number densities of dust grains as a function of the planetocentric distance. The number density has a maximum (about $3 \times 10^{3 \pm 1.5}$ km^{-3} for grains with radii >0.3 μm) near the orbit of Europa and gently decreases outward from Jupiter, dying away to nearly one order of magnitude smaller value at Callisto's orbit. Between the orbits of Europa and Ganymede the overwhelming majority of grains is supplied by Europa. Farther out, Ganymede grains make the largest contribution. The Callisto particles are a minor part of dust everywhere in the ring. Profiles of the partial rings formed by grains with different minimum sizes have similar shape. Of course, the larger the minimum size considered, the lower the absolute number density level.

[38] The modeling results allow us to estimate the optical depth of the ring. We use the calculated number densities of the grains in the size intervals [0.3, 0.6], [0.6, 1.0], and >1.0 μm (Figure 8b) and assume the partial rings to be vertically uniform with the height determined by the size-dependent typical inclinations (like those depicted in the bottom panels of Figure 3 for Europa 0.3-μm-sized grains). This gives the estimate of ring's maximum normal geometrical optical depth near the Europa orbit of $\tau \sim 10^{-9}$. Therefore the ring is much fainter than the main Jovian ring ($\tau \sim 10^{-6}$) and gossamer rings ($\tau \sim 10^{-7}$) [*Burns et al.*, 1999] and is not detectable by remote sensing. Besides, an extremely low optical depth rules out a possibility that the ring particles, striking the Galilean moons, efficiently create secondary ejecta and thereby maintain the ring, the so-called self-sustained scenario first proposed by *Hamilton and Burns* [1994] for the saturnian E ring and by *Sasaki* [1994] for the putative dust belts of Mars. It also clearly shows that mutual collisions of grains in the ring are unimportant for the dust budget and dynamics.

3. Galileo Dust Measurements

[39] Now we compare the modeling results with spacecraft data. The Galileo dust detector is a multicoincidence impact ionization dust detector which has been calibrated for grain impact velocities between 2 and 70 km s^{-1} and grain masses between 10^{-6} to 10^{-16} g [*Grün et al.*, 1992, 1995]. The instrument is identical to the dust detector on board Ulysses. For each impact onto the sensor target, three independent measurements of the impact-created plasma cloud are used to derive the impact speed and the mass of the impacting grain. Impact events are classified into four quality classes and six ion collector charge amplitude ranges (AR) [*Grün et al.*, 1995; *Krüger et al.*, 1999b, 2001]. Here we consider class 3 and denoised [*Krüger et al.*, 1999c] class 2 data ("true dust impacts"). In the Jovian environment the other classes contain mostly noise events. Class 3 impacts have three charge signals, whereas only two are required for a class 2 event. Apart from a missing third charge signal, there is no physical difference between dust impacts categorized into classes 3 and 2.

[40] In addition, we only consider impact events in amplitude range AR2. The AR1 events are not included, because the majority of these events were caused by impacts of tiny 10-nm-sized stream particles originating from Io's volcanoes [*Graps et al.*, 2000], which are not the subject of this paper and which cannot be easily separated from the impacts of larger grains in the same amplitude range. Besides, only for a small fraction of impacts in this charge amplitude range has the complete information necessary for further analysis been recorded. Amplitude ranges AR3 and higher are discarded as well, because these are dominated by impacts of dust grains in retrograde orbits [*Thiessenhusen et al.*, 2000], which are not compatible with ejecta from the Galilean moons.

[41] Galileo is a dual-spinning spacecraft with an antenna pointing antiparallel to the positive spacecraft spin axis. During most of the orbital tour around Jupiter the antenna points toward

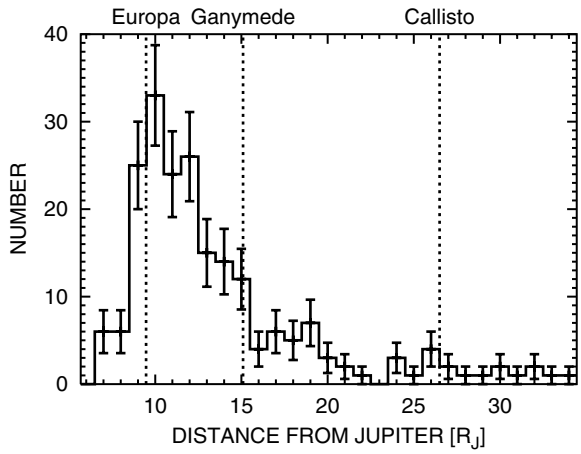

Figure 9. Number of particles detected by Galileo in the amplitude range AR2 as a function of distance from Jupiter.

Earth. The dust sensor is mounted on the spinning section of the spacecraft, and the instrument's sensor axis is offset by an angle of 60° from the spin axis (i.e., from the antiantenna pointing direction; an angle of 55° has been erroneously stated before [see *Krüger et al.*, 1999c]). The dust instrument has a 140°-wide field of view. During one spin revolution of the spacecraft the dust sensor scans the complete hemisphere opposite to the direction of the antenna. Dust particles which arrive from within 10° of the positive spacecraft spin axis can be sensed at all rotation orientations of the spacecraft, while those which arrive at angles between 10° and 130° can only be sensed over a limited range of rotation orientations. For a detailed description of the detection geometry the reader is referred to *Grün et al.* [1998].

[42] Figure 9 depicts the number of particles detected by Galileo at different distances from Jupiter. The histograms have been constructed by counting, in a given histogram bin, the number of AR2 events for which their complete set of measured impact parameters (charge signals, rise times, etc.) has been transmitted to Earth. Particles detected during the close flybys of Galileo at the Galilean satellites [*Krüger et al.*, 1999d] have been removed from the number distribution. The numbers of particles subtracted are 13 for Europa, 6 for Ganymede, and 2 for Callisto. These numbers do not represent the complete number of satellite particles detected because here we do not consider AR1 and AR3 to AR6, which also contain satellite particles.

[43] The numbers shown in Figure 9 cover the dust impacts detected with the Galileo dust detector between April 1996 (the second half of the J0 orbit) and June 2001 (C30 orbit), 208 events in total. In this time period, nearly all perijoves of Galileo's orbit were at about 9–10 R_J (Jovian radii) from Jupiter, i.e., close to the orbit of Europa, the apojove being from 70 to 150 R_J. The region inside ~9 R_J was sampled by Galileo only during its initial approach to Jupiter in December 1995 [*Grün et al.*, 1996] and then starting from the second half of 1999, near the perijoves of the C20 and later orbits. Besides, the sensitivity of the Galileo DDS to particles in prograde orbits was quite low. This results in a much smaller number of impacts below 9 R_J. Furthermore, data from the initial flyby of Galileo at Jupiter in December 1995, which cover distances down to 4 R_J, are not complete because of Galileo's low data transmission capability. Gaps in this data set also occur because the dust instrument was not operated continuously to save it from the hazards of Jupiter's high-radiation environment [*Krüger et al.*, 1999b]. All this makes the data for the region between 4 and 9 R_J rather uncertain. The region within 4 R_J from Jupiter was not sampled by Galileo at all. For these reasons, in this paper we do not analyze the distribution below ~9 R_J (i.e., within Europa's orbit).

[44] The numbers of detected events were converted to number densities of dust grains at different distances from Jupiter as described by *Thiessenhusen et al.* [2000]. We reproduce here the main points of the numerical procedure.

[45] First, we calculated, for different points along the spacecraft trajectory, the spin-averaged sensitive area of the Galileo DDS with respect to grains in prograde circular orbits. To this end, we took the velocity vector of Galileo at a given time instant, calculated the velocity vector a circular prograde grain would have at the same point, and subtracted both vectors to get the impact velocity vector of the grain relative to the spacecraft. The angle between this vector and the negative spin axis of Galileo (direction toward the Earth) is the so-called impact angle ϕ. The effective sensitive area of the detector $A_S(\phi)$, averaged over the Galileo rotation period, was then computed (see Figure 11 of *Krüger et al.* [1999c] or right panel of Figure 2 of *Thiessenhusen et al.* [2000]).

[46] For each distance bin the number of detected particles was divided by three quantities: the mean effective sensitive area in that bin (the maximum value of A_S is ~235 cm^2 for $\phi \approx 55°$), the mean impact speed of the grains in prograde circular orbits there (typically ~7 km s^{-1}), and the total time Galileo spent in the bin (typically about a week in a bin with a width of 1 R_J).

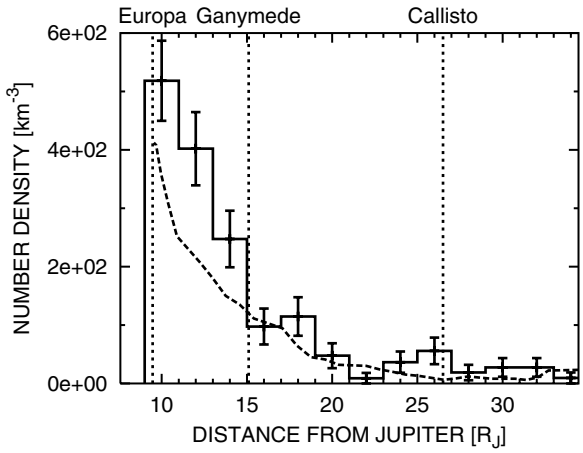

Figure 10. Radial profile of number density constructed from the measurements of Galileo spacecraft (solid line with error bars). Dashed line is the profile from *Thiessenhusen et al.* [2000] (right bottom panel of their Figure 10).

[47] This procedure allows for a number of effects. For instance, the impact velocity depends on the orbit geometry of the impacting grain and the spacecraft position [*Thiessenhusen et al.*, 2000, Figure 5]. In addition, the detection geometry and hence the detector sensitive area changed when Galileo approached Jupiter and most notably around perijove, affecting one or two innermost bins. Furthermore, the line of apsides of Galileo's orbit shifted by more than 90° with respect to the Earth direction during the period 1996–1999, which led to a gradual variation in the detection geometry from orbit to orbit [see *Thiessenhusen et al.*, 2000, Figure 8].

[48] The resulting number density profile is shown in Figure 10. For comparison, the dashed line displays number densities from *Thiessenhusen et al.* [2000], obtained from the first 15 orbits of Galileo with the same data processing procedure. Except for some local variations, the two profiles look similar. The latter profile is smoother because sliding averages over one day were used there.

[49] The histogram in Figure 10 directly compares with theoretical profiles depicted in the lowest panel of Figure 8. The number density profile derived from the data (Figure 10) is similar in shape to the profiles predicted by the model (Figure 8). Some differences can be attributed mainly to a number of assumptions made in the modeling (e.g., using a constant grain surface potential of +5 V for ejecta from all three moons).

[50] The absolute values of the number density suggested by the model are several times higher than those derived from the data. This is certainly an acceptable discrepancy, because we estimated uncertainties of the dust production rates to be at least a factor of 30 (section 2.1). Nevertheless, to make a comparison more accurate, we have to find out with which of the three curves in Figure 8 b the histogram of Figure 10 should be compared. These curves give the number densities of particles with radii above 0.3, 0.6, and 1.0 μm, or about 10^{-13}, 10^{-12}, and 10^{-11} g in terms of masses. Remember that the least of these values, 0.3 μm (or ~10^{-13} g), was taken because it corresponds to the sensitivity threshold that the Galileo DDS had during the flybys of the Galilean satellites [*Krüger et al.*, 2000]; we used these data in section 2.1 to set up the initial conditions for the ring modeling. The detector threshold depends on the mean impact speed, which was nearly the same during the Galilean moon flybys (~8 km s^{-1} [see *Krüger et al.*, 2000]) and during the measurements in the ring (~7 km s^{-1}). At a glance, this suggests that the number densities in Figure 10 refer to the grains >0.3 μm (>10^{-13} g), implying comparison with the solid line in Figure 8. In that case, the

absolute values coming from the data analysis would be 7 times smaller than those predicted by the theory.

[51] However, the data analysis for the satellite flybys was performed by taking into account all amplitude ranges, including AR1, whereas the ring data were processed without AR1. The reason was the necessity to eliminate impacts of Jovian stream particles that dominate AR1. In the first case, a reliable method exists to get rid of the stream particles by analyzing the geometry of impacts [*Krüger et al.*, 1999d, 2000], whereas in the second case no method has been found so far to identify and exclude this "contamination" from the AR1 range. The noninclusion of AR1 in the ring data processing automatically means a higher detector threshold. That is, the profile shown in Figure 10 probably refers to larger grains. According to estimates of *Thiessenhusen et al.* [2000], grains detected at AR2 near the perijoves may have had typical radii of $\approx$0.6 μm (masses $\sim 10^{-12}$ g) and not $\approx$0.3 μm (masses $\sim 10^{-11}$ g). Farther out from Jupiter, the radii/masses of AR2 grains may have been yet larger. If this is true, the histogram in Figure 10 should be compared to the dashed or even dotted line in Figure 8b and not the solid line, which would mitigate the discrepancy substantially. A direct check of calibrated masses of the detected grains in the data set that we made supports this expectation: the mean calibrated mass is $\approx 1.4 \times 10^{-11}$ g. We emphasize again that this discussion affects just a normalization factor (absolute value of the number density) and does not influence our main conclusions.

4. Conclusions and Discussion

[52] The main conclusion of this paper is that the Galilean satellites of Jupiter are likely to be efficient suppliers of dust for the Jovian system through the impact ejection mechanism. Our dynamical analysis shows that the dust grains from a few tenths of micrometers to $\sim$10 μm in size, leaving the satellites' spheres of influence, are likely to stay in bound orbits about Jupiter for tens of years, forming an ethereal dust ring between the orbits of the source moons. The gross features of the ring derived from the model seem to be in a general agreement with the data of the dust detector aboard the Galileo spacecraft. Absolute number densities of dust predicted by the model and coming from the data analysis agree to an accuracy of one order of magnitude. Also, the spatial variation of the number density suggested by the model is similar to that derived from the data.

[53] The extremely broad tenuous ring of debris is the first ring known to be formed by lunar-sized moons. To escape from the massive source moons, the dust ejecta must have initial speeds in excess of 2 km s^{-1}. Thus our analysis provided indirect evidence for the existence of high-speed ejecta from hypervelocity impacts into ice. This falls in agreement with recent laboratory impact experiments. For hypervelocity impacts into water ice, ejecta speeds of up to 0.6 km s^{-1} [*Frisch*, 1992] have been measured. Ejecta as fast as $\sim$2 km s^{-1} have been experimentally detected as well, although for regolith targets [*Yamamoto and Nakamura*, 1997]. These results have been idealized somewhat and should be applied to the ejecta from real satellites with some care. For instance, nongravitational forces have been neglected in our analysis of the dust dynamics in the vicinity of the source moons (section 2.1). Although we expect their effects to be small, they may nevertheless be noticeable [*Krüger et al.*, 2000].

[54] Unfortunately, it will be difficult to gain more insight into the properties of the ring. Theoretical analysis is hampered by poor knowledge of the impact ejection mechanism and mechanical properties of the satellite surfaces and by large uncertainties in the physical properties of dust grains and plasma environment. Furthermore, important features expected from the theory, such as time variability, spatial asymmetry of the ring (Figure 7), its vertical extension, or mass/size distribution of its particles, cannot be checked observationally at present because of the scarcity of the Galileo data and difficulties of the data reduction. Some additional data may come from the Galileo DDS in 2001–2003, while the Cassini spacecraft did not pass Jupiter close enough to assist. We estimate the ring's maximum normal optical depth near the Europa orbit to be $\tau \sim 10^{-9}$, which makes it far too tenuous to detect from current ground- or space-based telescopes.

[55] Another spacecraft, Ulysses, has also detected a small number of "big" impacts (events in amplitude ranges AR2 to AR6) during its Jupiter flyby in 1992: four impacts occurred around Europa's orbit, three outside the orbit of Ganymede, and two particles hit the detector outside Callisto's orbit. Despite Ulysses' highly inclined planetocentric orbit during Jupiter flyby, in the region between about 7 and 40 R_J its latitude with respect to the Jupiter's equatorial plane did not exceed ±35°. This is close to the vertical extension of the dust ring predicted by the model (see, e.g., the bottom panel of Figure 5). Therefore these events are compatible with being impacts of the ring particles.

[56] Interestingly, some evidence for the dust ring in the region of the Galilean moons can already be found in early measurements of the Pioneer 10 and 11 spacecraft. These spaceprobes carried arrays of pressurized cells, acting as low-sensitivity dust detectors with a threshold of about 10^{-9} to 10^{-8} g, or about 10 μm in terms of sizes. Twelve meteoroid penetrations have been detected by the Pioneers inside 45 R_J, three of which occurred just outside the Europa orbit and two of which occurred between the orbits of Ganymede and Callisto [*Humes*, 1976] (see also a discussion by *Zook and Su* [1982]).

[57] Some of the impacts onto the Galileo dust detector analyzed here (i.e., in the amplitude range AR2) could have been caused by grains of a different origin. However, interstellar, interplanetary, or Edgeworth-Kuiper belt particles, as well as possible ejecta from the outer retrograde moons, may be responsible only for a minor fraction of the impact events, and so mostly beyond the Callisto orbit, simply because their number densities of $\sim 10^1$, $\sim 10^0$, and $\sim 10^{-1}$ km^{-3}, respectively [*Colwell et al.*, 1998], are too low to account for the number densities we derive from the Galileo data inside the orbit of Callisto ($\gtrsim 10^2$ km^{-3}). Furthermore, these populations of dust would exhibit a differential radial distribution of the number density.

[58] In the same region, Galileo has also detected a number of impacts in higher amplitude ranges from AR3 to AR6, which we have not included in our analysis. Most of these impact events were attributed to particles on retrograde orbits [*Colwell et al.*, 1998; *Thiessenhusen et al.*, 2000]. Grains on retrograde orbits can hardly be explained by the ejection process from the Galilean moons, and they are most likely captured interplanetary grains [*Colwell et al.*, 1998]. However, their number density is probably four times smaller than that of the prograde particles [*Thiessenhusen et al.*, 2000], and they make only a minor contribution to the overall population of dust in the ring between the Galileans.

[59] The distribution of dust both outside $\sim$35 R_J and inside Europa's orbit is still unclear. Although Galileo has detected a small number of dust impacts at larger distances, up to $\sim$300 R_J, no interpretation to these events (interplanetary grains, ejecta from outer moons, etc.) has been given so far. Paucity of the data is complemented by the complexity of the physics in this region, close to the boundary of the Jovian magnetosphere. As far as continuation of the ring inward is concerned, Galileo traversed the region from Europa's orbit down to the orbit of Io (i.e., $\sim$9.5–5.9 R_J from Jupiter) several times during the period analyzed here, between October 1999 (I24 orbit) and February 2000 (I27). Owing to the high radiation levels close to Jupiter, the dust data collected there have to be processed in a different way to clearly distinguish dust impacts from noise events. In addition, the dust instrument shows radiation-related aging effects which lead to a change in the noise characteristics and the instrument sensitivity. These effects have to be taken into account when comparing data over a long

time period. The analysis of these data is ongoing and will be the subject of a future paper. Preliminary analysis, however, indicates an increase in the dust density towards the orbit of Io. Data from six more traverses between August 2001 (orbit I31) and January 2002 (orbit I33) are expected. Finally, in the end of 2002, Galileo may fly down to 2 R_J, entering the gossamer rings that extend to at least 3.5 R_J from Jupiter's center [*Ockert-Bell et al.*, 1999]. A combined analysis of Galileo's in situ measurements together with remote-sensing data by Galileo's cameras will open the unique opportunity to study the formation process of these dusty planetary rings.

[60] **Acknowledgments.** We appreciate useful discussions with Mihály Horányi and Frank Spahn. A.V.K. thanks his colleagues from Heidelberg for funding his stay at MPIK. Part of this work was done during A.V.K.'s Alexander-von-Humboldt fellowship at Max-Planck-Institut für Aeronomie (Katlenburg-Lindau, Germany). A.V.K.'s, K.U.T.'s, and H.K.'s work has been supported by the Deutsches Zentrum für Luft- und Raumfahrt (DLR) and the Deutsche Forschungsgemeinschaft (DFG). D.P.H. is grateful for support received from NASA and NSF.

References

Asada, N., Fine fragments in high-velocity impact experiments, *J. Geophys. Res.*, *90*, 12,445–12,453, 1985.

Burns, J. A., P. L. Lamy, and S. Soter, Radiation forces on small particles in the solar system, *Icarus*, *40*, 1–48, 1979.

Burns, J. A., M. R. Showalter and G. E. Morfill, The ethereal rings of Jupiter and Saturn, in *Planetary Rings*, edited by R. Greenberg and A. Brahic, pp. 200–272, Univ. of Ariz. Press, Tucson, 1984.

Burns, J. A., M. R. Showalter, D. P. Hamilton, P. D. Nicholson, I. de Pater, M. E. Ockert-Bell, and P. C. Thomas, The formation of Jupiter's faint rings, *Science*, *284*, 1146–1150, 1999.

Colwell, J. E., M. Horányi, and E. Grün, Capture of interplanetary and interstellar dust by the Jovian magnetosphere, *Science*, *280*, 88–91, 1998.

Dobrovolskis, A. R., J. L. Alvarellos and K. Zahnle, A dynamical survey of the Jovian system, paper presented at the 32nd DPS meeting, Am. Astron. Soc., Pasadena, Calif., 2000.

Everhart, E., An efficient integrator that uses Gauss-Radau spacing, in *Dynamics of Comets: Their Origin and Evolution*, edited by A. Carusi and G. B. Valsecchi, pp. 185–202, D. Reidel, Norwell, Mass., 1985.

Frisch, W., Hypervelocity impact experiments with water ice targets, in *Hypervelocity Impacts in Space*, edited by J. A. M. McDonnell, pp. 7–14, Univ. of Kent, Canterbury, England, UK, 1992.

Graps, A. L., E. Grün, H. Svedhem, H. Krüger, M. Horányi, A. Heck, and S. Lammers, Io as a source of the Jovian dust streams, *Nature*, *405*, 48–50, 2000.

Grün, E., H. Fechtig, M. S. Hanner, J. Kissel, B.-A. Lindblad, D. Linkert, D. Maas, G. E. Morfill, and H. A. Zook, The Galileo dust detector, *Space Sci. Rev.*, *60*, 317–340, 1992.

Grün, E., M. Baguhl, H. Fechtig, D. P. Hamilton, J. Kissel, D. Linkert, G. Linkert, and R. Riemann, Reduction of Galileo and Ulysses dust data, *Planet. Space Sci.*, *43*, 941–951, 1995.

Grün, E., et al., Dust measurements during Galileo's approach to Jupiter and Io encounter, *Science*, *274*, 399–401, 1996.

Grün, E., et al., Galileo observes electromagnetically coupled dust in the Jovian magnetosphere, *J. Geophys. Res.*, *103*, 20,011–20,022, 1998.

Hamilton, D. P., Motion of dust in a planetary magnetosphere — Orbit-averaged equations for oblateness, electromagnetic, and radiation forces with application to Saturn's E ring, *Icarus*, *101*, 244–264, 1993.

Hamilton, D. P., and J. A. Burns, Ejection of dust from Jupiter's gossamer ring, *Nature*, *364*, 695–699, 1993.

Hamilton, D. P., and J. A. Burns, Origin of Saturn's E ring: Self-sustained, naturally, *Science*, *264*, 550–553, 1994.

Hamilton, D. P., and A. V. Krivov, Circumplanetary dust dynamics: Effects of solar gravity, radiation pressure, planetary oblateness and electromagnetism, *Icarus*, *123*, 503–523, 1996.

Horányi, M., Charged dust dynamics in the solar system, *Annu. Rev. Astron. Astrophys.*, *34*, 383–418, 1996.

Horányi, M., J. A. Burns, and D. P. Hamilton, The dynamics of Saturn's E ring particles, *Icarus*, *97*, 248–259, 1992.

Horányi, M., G. Morfill, and E. Grün, The dusty ballerina skirt of Jupiter, *J. Geophys. Res.*, *98*, 221–245, 1993.

Humes, D. H., The Jovian meteoroid environment, in *Jupiter: Studies of the Interior, Atmosphere, Magnetosphere and Satellites*, pp. 1052–1067, Univ. of Ariz. Press, Tucson, 1976.

Johnson, R. E., J. W. Boring, C. T. Reimann, L. A. Barton, J. W. Sieveka, J. W. Garrett, K. R. Farmer, W. L. Brown, and L. J. Lanzerotti, Plasma ion-induced molecular ejection on the Galilean satellites — Energies of ejected molecules, *Geophys. Res. Lett.*, *10*, 892–895, 1983.

Kato, M., Y. Iijima, M. Arakawa, Y. Okimura, A. Fujimura, N. Maeno, and H. Mizutani, Ice-on-ice impact experiments, *Icarus*, *113*, 423–441, 1995.

Krivov, A. V., and D. P. Hamilton, Martian dust belts: Waiting for discovery, *Icarus*, *128*, 335–353, 1997.

Krüger, H., E. Grün, A. Graps, and S. Lammers, Observations of electromagnetically coupled dust in the Jovian magnetosphere, *Astrophys. Space Sci.*, *264*, 247–256, 1999a.

Krüger, H., et al., Three years of Galileo dust data, II, 1993 to 1995, *Planet. Space Sci.*, *47*, 85–106, 1999b.

Krüger, H., E. Grün, A. Heck, and S. Lammers, Analysis of the sensor characteristics of the Galileo dust detector with collimated Jovian dust stream particles, *Planet. Space Sci.*, *47*, 159–172, 1999c.

Krüger, H., A. V. Krivov, D. P. Hamilton, and E. Grün, Detection of an impact-generated dust cloud around Ganymede, *Nature*, *399*, 558–560, 1999d.

Krüger, H., A. V. Krivov, and E. Grün, A dust cloud of Ganymede maintained by hypervelocity impacts of interplanetary micrometeoroids, *Planet. Space Sci.*, *48*, 1457–1471, 2000.

Krüger, H., et al., One year of Galileo dust data from the Jovian system: 1996, *Planet. Space Sci.*, *49*, 1285–1301, 2001.

Lamy, P. L., Interaction of interplanetary dust grains with the solar radiation field, *Astron. Astrophys.*, *35*, 197–207, 1974.

Lieske, J. H., Theory of motion of Jupiter's Galilean satellites, *Astron. Astrophys.*, *56*, 333–352, 1977.

Ockert-Bell, M. E., J. A. Burns, I. J. Daubar, P. C. Thomas, J. Veverka, M. A. S. Belton, and K. P. Klaasen, The structure of Jupiter's ring system as revealed by the Galileo imaging experiment, *Icarus*, *138*, 188–213, 1999.

Sasaki, S., Martian dust tori formation: Ejecta at collision of torus particles with the satellite can sustain the dust abundance, in *Proceedings of the 27th ISAS Lunar and Planetary Symposium*, edited by M. Shimitzu and M. Mizutani, pp. 47–50, 1994.

Schaffer, L. E., and J. A. Burns, The dynamics of weakly charged dust: Motion through Jupiter's gravitational and magnetic fields, *J. Geophys. Res.*, *92*, 2264–2280, 1987.

Showman, A. P., and R. Malhotra, The Galilean satellites, *Science*, *286*, 77–84, 1999.

Thiessenhusen, K.-U., H. Krüger, F. Spahn, and E. Grün, Large dust grains around Jupiter — The observations of the Galileo dust detector, *Icarus*, *144*, 89–98, 2000.

Yamamoto, S., and A. M. Nakamura, Velocity measurements of impact ejecta from regolith targets, *Icarus*, *128*, 160–170, 1997.

Zook, H. A., and S.-Y. Su, Dust particles in the Jovian system, *Lunar Planet. Sci.*, *XIII*, 893–894, 1982.

A. V. Krivov, A G "Nichtlineare Dynamik," Institut für Physik, Universität Potsdam, Postfach 601553, 14415 Potsdam, Germany. (krivov@agnld.uni-potsdam.de)

E. Grün and H. Krüger, Max-Planck-Institut für Kernphysik, Postfach 103980, 69029 Heidelberg, Germany. (Eberhard.Gruen@mpi-hd.mpg.de; Harald.Krueger@mpi-hd.mpg.de)

D. P. Hamilton, Department of Physics and Astronomy, University of Maryland, College Park, MD 20742-2421, USA. (hamilton@astro.umd.edu)

K.-U. Thiessenhusen, Humboldt-Universität zu Berlin, Charité, Institut für Biochemie, Monbijoustrasse 2, 10117 Berlin, Germany. (kai-uwe.thiessenhusen@charite.de)